

A COMPLEXITY-BRIGHTNESS CORRELATION IN GAMMA RAY BURSTS

BORIS STERN^{1,2}, JURI POUTANEN², AND ROLAND SVENSSON²

Received 1997 October 13; accepted 1998 August 3

ABSTRACT

We observe strong correlations between the temporal properties of gamma ray bursts (GRBs) and their apparent peak brightness. The strongest effect (with a significance level of $\sim 10^{-6}$) is the difference between the brightness distributions of simple bursts (dominated by a single smooth pulse) and complex bursts (consisting of overlapping pulses). The latter has a break at a peak flux of $\sim 1.5 \text{ ph cm}^{-2} \text{ s}^{-1}$, while the distribution of simple bursts is smooth down to the BATSE threshold. We also observe brightness dependent variations in the shape of the average peak aligned time profile (ATP) of GRBs. The decaying slope of the ATP shows time dilation when comparing bright and dim bursts while the rising slope hardly changes. Both slopes of the ATP are deformed for weak bursts as compared to strong bursts. The interpretation of these effects is simple: a complex burst where a number of independent pulses overlap in time appears intrinsically stronger than a simple burst. Then the BATSE sample of complex bursts covers larger redshifts where some cosmological factor causes the break in the peak brightness distribution. This break could correspond to the peak in the star formation rate that was recently shown to occur at a redshift of $z \sim 1.5$.

Subject headings: gamma rays: bursts – gamma rays: observations – methods: statistical

1. INTRODUCTION

Do the temporal properties of GRBs have systematic trends that are dependent on brightness? The most intensively discussed and studied trend is the time dilation of weak bursts relative to strong bursts. The attention to the time dilation effects is due to its possible cosmological interpretation (Paczynski 1992). The results of time dilation measurements differ for different groups: Norris et al. (1994), Fenimore & Bloom (1995), and Stern (1996) found time dilation, while Mitrofanov et al. (1996) and Lee & Petrosian (1997) did not find any significant effect.

Positive detections of time dilation are consistent with the simplest assumption that weak events are just redshifted (and therefore stretched) analogs of strong events. However, in the work of Stern, Poutanen & Svensson (1997, hereafter SPS97), it was demonstrated that the situation is more complicated. Weak events are not only longer on average, but they are also more asymmetric on average. Furthermore, their average peak aligned time profile (ATP) has a different shape as compared to strong events. This difference can be quantified in terms of different stretched exponential indices.

Such brightness dependent correlations are in contradiction with a straightforward interpretation of the temporal stretching as being due to cosmological time dilation. On the other hand, these correlations can easily be interpreted in terms of correlations between temporal properties and *intrinsic peak luminosity*. Indeed, GRBs are composed of individual asymmetric pulses with fast rise and slower exponential decay (FREDs). The ATP of simple GRBs consisting of one pulse (or a few pulses) is on average more asymmetric than the ATP for complex GRBs where a chaotic bunch of overlapping pulses can produce an arbitrary time profile and the asymmetry related to the individual pulses is washed out. If we assume that different elementary pulses originate in different regions being associated with local events in the course

of a global event, then the amplitudes of elementary pulses with overlapping arrival time sum up. Therefore, complex bursts consisting of many overlapping pulses are intrinsically brighter than simple events. A direct morphological classification performed by SPS97 confirmed this interpretation: complex bursts show systematically larger peak fluxes than simple GRBs.

Although such correlations are natural in intrinsic peak luminosity, we, however, observe them in a narrow range (within one decade) of *apparent* peak brightness (i.e., peak count rate). This means that the distribution of GRBs over luminosity distance differs significantly from a power law. (In the case of a power law, intrinsically strong and intrinsically weak GRBs would be blended in the same proportion at any apparent brightness.) These correlations can put additional constraints on the spatial distribution of the GRB sources.

This work follows SPS97 in its main objectives. A larger statistics of GRBs is used, and, most importantly, the procedure of discriminating between simple and complex bursts is formalized and made more efficient. Due to the latter improvement, the direct test for a complexity - peak brightness correlation gives a very significant and meaningful result, which is described in § 3. Then, in § 4, we describe the results of our studies of the ATP shape as a function of brightness. These studies show further effects which are also associated with the complexity - brightness correlation. In § 5, we present a model example demonstrating how the above correlations could occur using simple assumptions and discuss the issue of the GRB intrinsic luminosity function. In the Appendices, we present a detailed description of the data analysis for the ATP study as well as a number of additional tests for possible systematic errors.

Some of the results presented here were also presented in a preliminary form in Stern, Svensson, and Poutanen (1997).

When using words “brightness”, “bright”, “dim”, “strong”, or “weak”, we always refer to the *apparent* peak brightness (peak flux or peak count rate), except in those cases when we clearly write *intrinsic*.

¹ Institute for Nuclear Research, Russian Academy of Sciences Moscow 117312, Russia

² Stockholm Observatory, SE-133 36 Saltsjöbaden, Sweden

2. DATA ANALYSIS

This work is based on the data in the publically available Compton Gamma-Ray Observatory data archive at Goddard Space Flight Center. Our sample includes bursts up to trigger number 6230 and contains 1395 events selected as useful for the complexity – brightness analysis and 1310 events being useful for the ATP study. We use 0.064 s and 1.024 s time resolution data from the Large Area Detectors (LAD). All the time profiles are constructed in 64 ms resolution with a 1024 ms resolution extension if necessary. All background fits are done using the 1024 ms data as they cover a wider time range including the pre-trigger history. We use the count rate summed over the four LAD energy channels covering the 25 – 1000 keV energy range, when studying the behavior of the ATP, as well as the count rate summed over channels 2–3 (50 – 300 keV) in our complexity – brightness analysis (see SPS97). Backgrounds were subtracted using linear fits. A visual scan of all triggered bursts was performed in order to select useful events and to set the fitting windows.

As a measure of peak brightness we use the peak flux, F_p , or the peak count rate, P , depending on the application. Peak fluxes in 64 ms time resolution from the current BATSE catalog (Meegan et al. 1998) were used when sorting bursts into brightness groups: this is a traditional measure which is more convenient when comparing results of different works. On the other hand, peak count rates have a more direct association with the trigger efficiency. Therefore, in § 3, we use our estimates of the 64 ms peak count rate as a measure of brightness instead of using the peak fluxes from the catalog. In order to reduce brightness dependent biases associated with Poisson noise, we developed a peak search scheme where each count rate excess over neighboring time intervals is tested for its statistical significance.

Important procedures of the data analysis and their tests are described in Appendix A.

3. DIFFERENT BRIGHTNESS DISTRIBUTIONS FOR SIMPLE AND COMPLEX BURSTS

It is comparatively easy to distinguish between complex and simple events for the bright GRBs. One can then introduce a numerical measure of complexity, e.g., the total length of up and down variations normalized to the peak count rate. Alternatively, one can count runs up and down and use their number to characterize complexity (Lestrade 1994). Unfortunately, such an approach fails when dealing with weak GRBs because of the Poisson noise which heavily dominates any of the measures mentioned above (various attempts to filter out the noise do not help).

The only possibility to extract a “simple” subpopulation from the weak burst population is to use the “canonical” shape of a single pulse, which is more or less identifiable by the human eye or by a χ^2 fit. The former approach was used by SPS97 in the form of a visual blind test. All events were rescaled to the same (low) brightness adding proper Poisson noise. Then each rescaled event was classified by three test persons as “simple” (a single FRED pulse), or as “complex” (not a FRED pulse), or “unresolved” (usually too short to be confidently identified). Then the peak count rate distributions for simple and complex GRBs were compared. Two of three test persons showed that complex GRBs are systematically brighter at a significance level exceeding 0.01, the third test person showed the same effect at a significance level of 0.1. We now present results using the χ^2 tests on a larger statistics

of GRBs.

3.1. The χ^2 Separation Between Simple and Complex Bursts

Unlike the visual test of SPS97, the χ^2 test is aimed at extracting events *dominated* by a single FRED pulse rather than consisting of a single FRED pulse. That is, the main peak was checked for how well it is fitted by the FRED’s pulse shape, while other smaller peaks not affecting the fit were allowed for an event to be qualified as “simple”. Pulses were fitted with the parameterization of Norris et al. (1996): $C_{r,d}(t) = C_p \exp(-[|t - t_{\max}|/\tau_{r,d}]^\nu)$, where ν was allowed to vary between 0.9 and 2.2, t_{\max} to vary within ± 3 seconds around a direct estimate of the peak position. The three parameters, the peak count rate, C_p , the rise time, τ_r , and the decay time, τ_d , were free. The fitting time interval was $(t_{\max} - 6\tau_r^{1/\nu}, t_{\max} + 6\tau_r^{1/\nu})$. The fit for each event was performed for 64, 128, 256, and 512 ms bins. The maximum value of χ^2 per degree of freedom (χ_m^2) for these four variants of binning was used for the classification. All events with a peak count rate > 55 counts/64 ms were tested (dimmer events were discarded), and all of them were rescaled to a peak count rate (in energy channels 2+3) of 55 counts/64 ms. All events with $\tau_r + \tau_d < 2$ s were discarded as the time resolution for short peaks at this small brightness is insufficient.

A visual examination of the fitting procedure showed that it is not perfect, but this is natural. Sometimes a bright GRB which looks as an apparently complex dense bunch of pulses gave a good χ^2 when rescaled to low brightness, and sometimes a GRB looking like a FRED had a bad χ^2 not satisfying the parameterization (in such cases no human intervention occurred, of course). Nevertheless, in 90% of the events the result of the χ^2 test coincided with the visual impression, so we conclude that the above parameterization and the whole procedure work satisfactorily. Typically, the largest χ_m^2 was obtained for the widest binning, 512 ms.

The number of resolved events for which the classification simple-complex was possible is 852 (of 1395 useful events). The distribution of χ_m^2 for these events is presented in Figure 1a. Note the striking difference in distributions for “fast risers” and “slow risers” which confirms that the test finds many really simple events among fast risers (which can be simple bursts) and almost none of them among slow risers (which should be complex bursts).

We found an apparent positive correlation between χ_m^2 and the peak count rate (the reason why we use the peak count rate instead of the peak flux as the measure for brightness is discussed below). We separated bursts by different thresholds χ_t^2 in χ_m^2 and compared peak count rate distributions for simple ($\chi_m^2 < \chi_t^2$) and complex ($\chi_m^2 > \chi_t^2$) events estimating their consistency levels with the Kolmogorov-Smirnov (KS) test. The results are presented in Figure 1b. We see that without applying the $\tau_d > \tau_r$ criterion we have a significance level for the complexity – brightness correlation of $\sim 3 \times 10^{-4}$ (i.e, a disproof of the null hypothesis that the brightness distributions for simple and complex bursts are the same), while applying the $\tau_d > \tau_r$ criterion the significance level is $< 10^{-6}$ (with the external value of 1.4×10^{-7}). Our final choice for the classification of a burst as “simple” is: $\tau_d > \tau_r, \chi_m^2 < 1.45$ (all other events satisfying $\tau_r + \tau_d > 2$ s are classified as complex).

3.2. Peak Count Rate Distributions for Simple and Complex GRBs

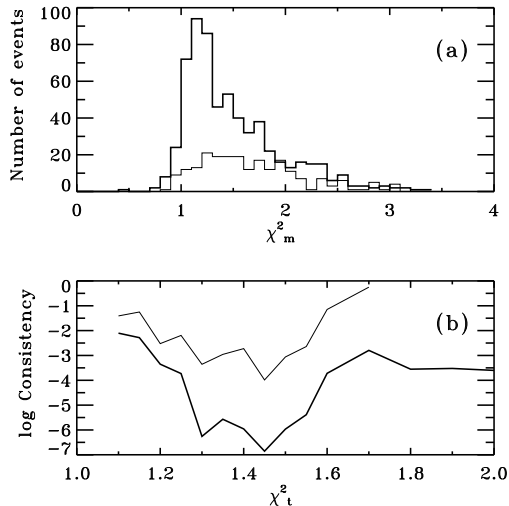


FIG. 1.— a) The reduced χ^2 distribution for the 852 “resolved” events with $\tau_r + \tau_d > 2$ s. Thick histogram: GRBs (626 events) with faster rise than decay ($\tau_r < \tau_d$). Thin histogram: GRBs (226 events) with slower rise than decay ($\tau_r > \tau_d$). b) The consistency level using the Kolmogorov-Smirnov criterion for the peak count rate distributions of simple ($\chi_m^2 < \chi_t^2$) and complex ($\chi_m^2 > \chi_t^2$) GRBs as a function of the χ_m^2 threshold χ_t^2 . Thick curve: the condition $\tau_r < \tau_d$ is applied when distinguishing simple and complex events. Thin curve: the condition $\tau_r < \tau_d$ is ignored.

We construct differential peak count rate distributions ($\log N - \log P$) for simple and complex events separately. These distributions corrected for the trigger efficiency (each class has its own efficiency) are presented in Figure 2. We plot the number of bursts as a function of peak count rate, while the values for the peak flux from the current BATSE catalog (Meegan et al. 1998) corrected for the spacecraft orientation, number of triggered detectors, and reflection from the atmosphere could be a better measure of brightness. The effect in the BATSE catalog peak flux distributions of simple and complex GRBs is similar: the KS test gives a consistency level of 10^{-5} when using 1024 ms peak fluxes and 10^{-7} for 64 ms peak fluxes. Unfortunately, it is much more difficult to estimate the trigger efficiency as a function of the peak flux. The trigger efficiency is a much sharper and better defined function of the peak count rate than of the peak flux. This simplifies the problem of correcting for the trigger efficiency when using peak count rate units.

Besides the trigger efficiency there exists a bias for the brightness dependent dead time for burst read-outs. (The trigger during read-out time is revised so that a new event brighter than the triggered event on a 64 ms time scale overwrites the first trigger while a weaker event will be lost.) The effect can be accounted for by discarding from the sample all events which overwrite a previous trigger. We found that the effect is small enough (only 5% of our events are “overwrites”). Moreover, the effect is almost the same for simple and complex events (within the statistical accuracy) and does not affect the difference in their distributions. In order to save the statistics, we work with the full sample of useful bursts.

The difference in the behavior of the $\log N - \log P$ distributions for the two classes of GRBs is striking. While the curve for simple events is consistent with a power law down to the trigger threshold, the complex class demonstrates an apparent break at a count rate exceeding the threshold by a factor of 3 – 5. If one shifts the “complex” distribution by a factor $1/k < 1$ discarding bursts moving below the threshold (i.e., $P/k < 55$ counts/64 ms) then the KS consistency level peaks at $k = 2.1$

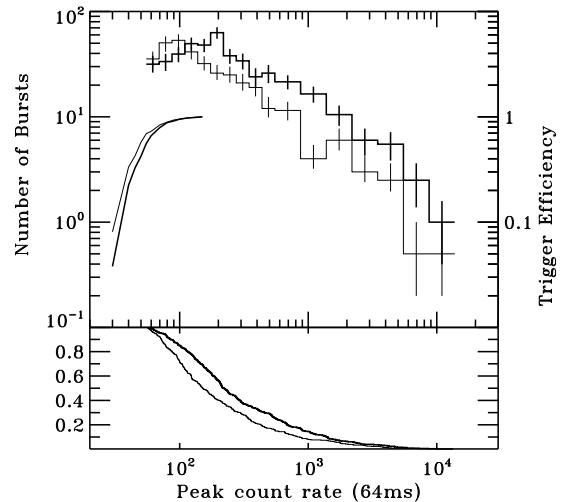


FIG. 2.— Differential peak count rate distributions for simple (thin histogram) and complex GRBs (thick histogram) corrected for the trigger efficiency (upper panel). The trigger efficiency for simple (thin curve) and complex (thick curve) bursts are plotted in the lower left corner. Lower panel gives the normalized cumulative distributions for simple GRBs (355 events) and complex bursts (497 events) used in the Kolmogorov-Smirnov test.

which can be interpreted as complex events being ~ 2 times brighter on average. This factor can be even larger depending on the behavior of the “simple” distribution below threshold.

The main difference in the count rate distributions is concentrated in the low count rate range and can be described as a relative deficit of complex bursts by a factor ~ 2 near threshold. The low count rate range may contain systematic biases (threshold effects) and we must estimate them before drawing any conclusions. We have no reason to suspect the rescaling procedure as being a source of bias as this procedure is trivial and one can exactly account for the variation of noise when we rescale bursts to the same brightness. Another possible bias can be associated with the errors of the background fits, but this bias has the opposite sign of the effect: weak bursts should give a higher χ^2 due to nonzero residuals outside of the peak. The visual classification of SPS97, which is less sensitive to rescaling and insensitive to the background subtraction, gave a similar result.

We also cannot suspect systematic errors in the estimates of the peak count rates. The reasonable linearity of these estimates is demonstrated in Appendix A (see Fig. 8 there). A correlation between complexity and the peak count rate estimates could exist but this is a 10% effect, while a factor 2 bias is required to account for the effect. A more serious source of systematic error could be a different trigger efficiency for simple and complex events. Indeed, slow risers, which have lower trigger efficiency, mostly belong to the complex sample. In order to verify this, we calculated the trigger efficiency separately for simple and complex events as described in Appendix A (the distributions in Fig. 2 as well as the significance levels given above are already corrected for different trigger efficiencies).

The efficiency for complex events is actually lower, e.g., at a peak count rate of 55 counts/64 ms it is 0.69 for simple events and 0.56 for complex events. Nevertheless, the difference is negligible compared to that required to explain the effect: at least a correction by a factor of two applied only to complex weak bursts is required to make the distributions consistent. We can hardly admit as explanation that it is the result of a huge unknown selective bias which affects only high

χ^2 bursts but does not affect low χ^2 events. We suggest that the upper curve in Figure 2, representing presumably intrinsically strong events, extends to larger cosmological distances, where some effect associated with high redshifts becomes important. Then, it is natural to suggest that the lower curve will show a similar behavior below the threshold.

Recently, Pendleton et al. (1997) found a similar effect that separating GRBs into subclasses affected their $\log N - \log P$ distribution. The presence of a hard tail in the spectrum (significant emission above 300 keV) was used as a criterion for separation. It is possible that the “no high energy” and “high energy” subclasses of Pendleton et al. correlate with our simple and complex groups, respectively.

In a cosmological scenario, it is natural to suggest that the intrinsically strong subpopulation of BATSE GRBs extends to $1 < z < 3$ where the Universe evolves strongly. The evolution at this epoch is clearly visible in the QSO redshift distribution (Hartwick & Schade 1990) and in the star formation rate curve (Madau et al. 1996; Abraham 1997). In the neutron star merging scenario (Blinnikov et al. 1984; Paczyński 1992), the GRB rate should be associated with the star formation rate (Lipunov et al. 1995; Prokhorov, Lipunov, & Postnov 1997). In this case, the break in the $\log N - \log P$ curve for complex GRBs should correspond to the peak in the star formation rate at $z \sim 1.5$. In the galactic halo model, a cutoff in the neutron star radial distribution could also account for the observed break.

Another interpretation is that the different $\log N - \log P$ distributions of simple and complex bursts could be associated with a possible existence of two different classes of events among the simple GRBs. One class could have a non-cosmological origin and therefore Euclidian $\log N - \log P$ distribution which when being added to the cosmological component could explain the effect. Extending the $\log N - \log P$ distribution using non-triggered bursts could provide the answer.

4. BRIGHTNESS DEPENDENT CORRELATIONS IN THE AVERAGE TIME PROFILE

After confidently observing a complexity – brightness correlation, the ATP – brightness correlation can be considered to be a direct consequence of the former. Nevertheless, the later still provides an independent confirmation of the correlation tendency, complete the picture, and is interesting in itself. For this reason, we present the latest results of our ATP studies together with a more detailed description than was given in SPS97.

4.1. On the Stretched Exponential Shape of the ATP

A stretched exponential (SE) shape of the ATP, $f(t) \equiv < F(t)/F_p > = \beta \exp[-|t/t_0|^\nu]$, was claimed by Stern (1996) for the decaying slope and was confirmed with successively higher statistics by Stern & Svensson (1996) and SPS97 (in the latter work, an SE shape of the rising slope of the ATP was also demonstrated). Both the rising and the decaying slopes of the ATP for the overall useful BATSE statistics (1310 events) are presented in Figure 3a. The high statistics demonstrates that the picture is more complicated than the idealized assumptions in SPS97. The rising and the decaying parts have not only different time constants but also different shapes (i.e., different SE indices, ν). The decaying ATP is perfectly described by an SE with $\nu = 0.37$, while the rising ATP is described by an SE with $\nu = 0.30$. Note that the whole “disorder” comes from weakest bursts. If we remove them, both the

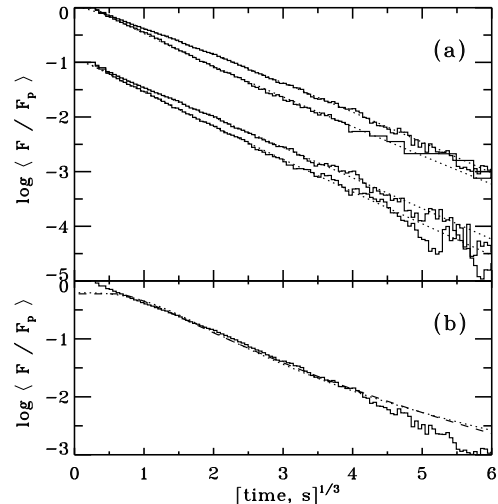


FIG. 3.— a) Rising and decaying slopes of the ATP with their stretched exponential fits. Upper set of curves: the full useful sample, 1310 GRBs; lower set of curves (shifted down for clarity): the 953 brightest GRBs. Rising slopes are steeper than the decaying for both cases. Dotted curves represent the best 3-parameter (β, ν, t_0) stretched exponential fit. Best fit values of ν for the whole sample are 0.30, 0.37 for the rising and decaying slopes, respectively. For the bright sample, $\nu \approx 0.33$, for both slopes. b) Examples of fits of the decaying ATP using other functions. Dotted curve: the parameterization of Mitrofanov et al. (1997), $f(t) = \beta[t_0/(t_0 + t)]^\alpha$; dashed curve: the one-sided log-normal distribution (see text)

rising and decaying ATPs are much closer to the “canonical” shape with $\nu = 1/3$ (Fig. 3a). The different ATP shape of the weakest bursts was noted by SPS97. The difference is significant and cannot result from the trigger selection effect. The interpretation of this fact is discussed below. For now we just note that:

- An SE shape with $\nu = 1/3$ for both slopes is still a good working hypothesis for stronger bursts.
- For the full sample, the SE indices of the rising and decaying ATPs differ. The difference is real and significant ($\sim 4\sigma$ effect). However, both ATPs are still described by SEs. We demonstrate below that the difference in ATP shapes is a natural consequence of the asymmetric shape of elementary pulses.

Let us now consider the issue of whether the stretched exponential shape of the ATP is just a successful fitting hypothesis among other comparable possibilities or if it is a natural intrinsic feature of the ATP?

The $\log f - \log t$ plot of the ATP does not resemble a power law in any time interval. Nevertheless, Mitrofanov, Litvak & Ushakov (1997) used a fitting expression with power law asymptotic, $f(t) = [t_0/(t_0 + t)]^\alpha$, to fit the ATP. Introducing a third parameter, the general multiplier β (i.e., $f(t) = \beta[t_0/(t_0 + t)]^\alpha$), the best fit for the decaying part of the ATP in the 0.125 - 216 seconds range gives $t_0 = 3.62$, $\alpha = 1.33$ with $\chi^2 = 128$ for 19 degrees of freedom (Fig. 3b) and with an unreasonably small value at $t = 0$: $f(0) = \beta = 0.62$. Since Mitrofanov et al. (1997) constructed the ATP in 1024 ms resolution (i.e., the $t < 1$ s region was lost) and only within the $t < 20$ s range, it is not surprising that they obtained a good fit in this narrow interval. However, for a wider time interval this parameterization is unacceptable.

Let us take as another example the log-normal distribution which is quite common in Nature. It has the wrong asymptotic at $t = 0$, but we correct this by setting $f(t) = \beta \exp(-\log^2(t/t_0)/2\sigma^2)$ at $t > t_0$ and $f(t) = \beta$ at $t < t_0$. This

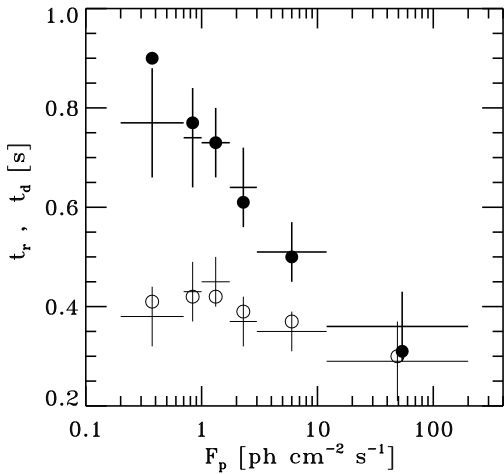


Fig. 4.— Time constants, $t_{r,d}$ (s), vs peak photon flux in 64 ms time resolution, F_p ($\text{ph cm}^{-2} \text{s}^{-1}$). The SE index, ν , was fixed to $1/3$. Upper and lower crosses represent results for the post-peak (decaying) and pre-peak (rising) ATPs, respectively. Error bars in $t_{r,d}$ correspond to the values in Table 5 in Appendix B. Error bars in photon flux represent the width of the brightness group. Open and filled circles represent best fit values for $t_{r,d}$ with ν fixed at 0.30 and 0.37 and rescaled with the factors $1/0.51$ and $1/1.6$ for the rising and decaying slopes, respectively.

semi-artificial expression fits the ATP in the same range as above with $\chi^2 = 89$ for 19 degrees of freedom (best fit parameters $t_0 = 0.20$ and $\sigma = 3.18$) and again with an unsatisfactory value at $t = 0$: $f(0) = \beta = 0.6$ (see Fig. 3b). For comparison, an SE fit of the same ATP gives $\chi^2 = 4.1$ at $\nu = 0.37$, $t_0 = 1.12\text{s}$, and $\beta = 1.04$. For the reasonableness of the χ^2 values, see Appendix B.

Probably, there is no 3-parameter expression which would fit the ATP on such a broad time interval except for the SE. Note, that our SE fit is in fact a “2.5-parameter” fit, i.e., the third parameter, the multiplier β , just accounts for the uncertainty associated with the first 64 ms bin of the ATP assumed to be close to 1. The best fit value of β is actually always close to 1 and therefore we do not give the β -values.

Summarizing the issue, we state that the stretched exponentiality of the ATP is probably not exact. However, with the existing statistics we do not see any statistically significant deviations. The SE is a natural distribution shape in very different classes of physical phenomena when a wide range of time scales are involved (Ching 1991; Jensen, Paladin, & Vulpiani 1992). Therefore we believe that our choice of SE as the fitting expression is not only efficient but also meaningful.

The procedures of measurement of the SE time constants of the ATP and estimates of statistical errors follow SPS97. They are described in more detail in Appendix B.

4.2. Time Constants of the ATP as a Function of Peak Flux

We use the following parameterization of the ATP: $f(t) = \beta \exp\left[-|t/t_{r,d}|^{\nu_{r,d}}\right]$, where $t_{r,d}$ and $\nu_{r,d}$ are the time constants and the SE indices of the rising and decaying ATP, respectively. In our studies of the ATP behavior, we use two kinds of SE fits. The first is the simultaneous fit of both ATP slopes with SEs of the same index, $\nu = 1/3$, and a common normalization factor β . This 3-parameter fit (t_r , t_d , and β) has the best statistical accuracy. The results of these SE fits are summarized in Table 1 and in Figure 4.

In comparison to the GRBs statistics used by SPS97 (912 events), the temporal stretching of the decaying slope

for weak events is now more pronounced and significant, $t_{d,9}/t_{d,7} = 1.89^{+0.68}_{-0.44}$ (90% confidence interval) comparing samples 9 and 7 (see Table 1). The corresponding rejection level for a null hypothesis (i.e., no temporal stretching) has now increased to 0.99995 (assuming a normal distribution for the deviations of the values). The temporal stretching of the rising slope also increased slightly, but this is still at a low significance level. The resulting variation of the asymmetry (the ratio t_d/t_r) slightly decreased. Comparing samples 1 and 9 we get: $(t_d/t_r)_{\text{dim}}/(t_d/t_r)_{\text{bright}} = 1.48^{+0.55}_{-0.32}$ (90% confidence interval). The significance level for this correlation remains the same as for the SPS97 sample, ~ 0.02 . The variation of $t_r + t_d$ with peak flux has a statistical significance of 4×10^{-4} ; the “dim/bright” ratio becomes $(t_r + t_d)_9/(t_r + t_d)_7 = 1.71^{+0.62}_{-0.38}$ (sample 9 compared to sample 7).

The results presented so far were obtained with a fixed SE index, $\nu = 1/3$. We now present a second fitting variant. As was mentioned above, the ATP for the whole sample indicates a larger ν for the decaying slope and a lower ν for the rising slope. Despite the fact that the difference results from the contribution of weak GRBs, it would be interesting to check the behavior of the time constants when ν is fixed to different values for the two slopes. Unfortunately, we cannot then use a common β for both slopes, as this would lead to unacceptable values of χ^2 . Therefore, we performed *independent* 2-parameter fits (β_r, t_r) and (β_d, t_d) for the two slopes setting $\nu_r = 0.30$, $\nu_d = 0.37$. (These fits give 20% larger statistical errors for the time constants as compared to the simultaneous 3-parameter fit.) With such a fit, t_r becomes systematically smaller (by a factor 0.51), and t_d systematically larger (by a factor 1.6). Such an effect on the time constants is due to the strong correlation $\nu - t_{r,d}$ (see Fig. 10 in Appendix B). These time constants rescaled by a factor $1/0.51$ and $1/1.6$ are shown in Figure 4. One sees that the behaviors of these time constants with peak flux are the same. The variation of the asymmetry, t_d/t_r , is even slightly larger than for the first fitting variant.

To test for spectral redshift of weak bursts as being the possible explanation of the asymmetry variation, we measured the asymmetry in separate LAD’s energy channels. If GRBs were more asymmetric at higher energies, then the spectral redshift of the softer, more symmetric, component to energies below the observational band could cause an asymmetry – brightness correlation. The results are presented in Table 2. One sees no tendency supporting such a hypothesis: GRBs have the same asymmetry in all channels.

A test for the presence of brightness dependent biases in these results is described in Appendix A. Only the weakest sample 6 is affected by the trigger selection bias and by Poisson noise. For this reason, sample 6 was excluded from the analysis of the brightness dependent correlations.

4.3. Variations of the Stretched Exponential Index with Peak Flux

Figure 5 presents the decaying and rising slopes for samples 1+2, 3+4, and 5+6. The stretched exponential indices for these samples are given in Table 3. Except for the apparent “time dilation” effect, the deformation of the weakest ATP is clearly visible. Partially, this deformation results from brightness dependent biases (short weak bursts have smaller trigger efficiency and the peak searching scheme is unable to find the sharp peaks of longer events, also see Fig. 9 in Appendix A). These biases suppress the ATP within 1 s from the

TABLE 1
TIME CONSTANTS OF THE AVERAGED TIME PROFILES (ATPs)

#	Peak flux	N	t_r	t_d	$t_r + t_d$	t_d/t_r	χ^2
1	12 – ∞	84	0.29±0.08	0.36±0.07	0.65±0.13	1.23 ±0.17	7.6
2	3 – 12	282	0.35±0.04	0.51±0.06	0.87±0.09	1.47 ±0.11	6.9
3	1.75 – 3	239	0.37±0.05	0.64±0.08	1.01±0.12	1.74 ±0.21	4.8
4	1 – 1.75	358	0.45±0.05	0.73±0.07	1.17±0.11	1.63 ±0.11	21
5	.7 – 1	196	0.43±0.06	0.74±0.10	1.17±0.15	1.70 ±0.15	22
6	0 – .7	151	0.38±0.06	0.77±0.11	1.15±0.17	2.00 ±0.20	29
7	7.5 – ∞	145	0.29±0.05	0.38±0.06	0.67±0.10	1.33 ±0.14	11
8	5 – ∞	209	0.29±0.04	0.41±0.05	0.71±0.09	1.40 ±0.12	9
9	.8 – 2.5	659	0.43±0.04	0.72±0.06	1.15±0.09	1.68 ±0.09	25

NOTE. — Time constants, t_r and t_d (s), are given for the stretched exponential simultaneous fit with $\nu = 1/3$ to the pre-peak and post-peak average time profiles, respectively. Peak fluxes in 64 ms resolution ($\text{ph cm}^{-2} \text{s}^{-1}$) are taken from the BATSE database and are measured in channels 2 and 3. N is the number of bursts in the given brightness interval. The fitting time interval is $0.5 < |t^{1/3}| < 5$. The errors and the χ^2 values (for 33 formal degrees of freedom) are estimated as described in Appendix B.

TABLE 2
TIME CONSTANTS MEASURED WITH $\nu = 1/3$ IN DIFFERENT ENERGY CHANNELS

Channel #	t_r	t_d	t_d/t_r
1	0.50	0.70	1.40
2	0.42	0.56	1.33
3	0.35	0.42	1.20
4	0.20	0.27	1.35
1 - 4	0.39	0.53	1.35

NOTE. — Time constants, t_r and t_d , of the averaged time profiles are given for the 280 brightest events in separate LAD energy channels. The value of the index ν was fixed at $1/3$. Relative errors for t_r and t_d are 12%, for t_d/t_r they are 8%.

peak while its effect beyond 1 s is not so strong.

TABLE 3
SE INDICES FOR THREE WIDE BRIGHTNESS GROUPS

#	Peak flux	N	ν_r	ν_d
1+2	3 – 200	366	0.338±0.027	0.322±0.026
3+4	1 – 3	597	0.316±0.020	0.359±0.023
5+6	0 – 1	347	0.252*	0.411±0.034
All	0-200	1310	0.300±0.017	0.371±0.021

NOTE. — ν_r, ν_d are best fit SE indices for the 3-parameter (free β, ν_r, t_r, t_d) fit in the $0.5 < |t^{1/3}| < 6$ interval.

* For sample 5+6, the fit was done in the $1 < |t^{1/3}| < 6$ time interval because of too strong ATP deformations within 1 second. Errors were not estimated.

The estimate of the significance level for the shape variation is difficult because trigger selection and Poisson biases give deformations of the same sign as (but still much smaller than) observed. SPS97 estimated the significance level of deformation of the decaying slope for the weakest sample as 0.05 after correcting for the above biases and possible error of the background subtraction. We do not make such an estimate here, because the deformations of the ATP must appear as a direct consequence of the much more significant complexity – brightness correlation described above.

5. ON THE ISSUE OF THE INTRINSIC LUMINOSITY FUNCTION

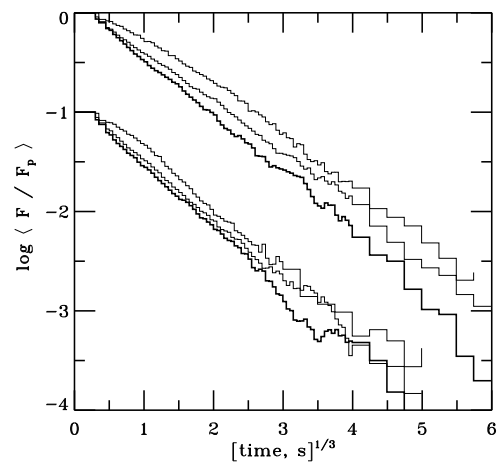


FIG. 5.— Decaying and rising slopes of the ATP for different brightness groups: strong (samples 1+2), medium (samples 3+4), and weak (samples 5+6). Rising slopes are shifted down for clarity. Stronger bursts have smaller time constants (slopes are steeper).

When separating GRBs into brightness groups using their peak fluxes, we assumed that the peak fluxes give us an approximate measure of the distance (a standard candle approximation). The fact that we see correlations between the shape of the ATP and apparent peak brightness tells us that the peak luminosity has a rather broad distribution and correlates with the ATP. What could serve as a better standard candle?

Some researchers suggest that the total energy fluence is a better standard candle than the peak luminosity (e.g. Petrosian & Lee 1996) arguing that this would be more physical. However, if we accept that something like the pulse avalanches of Stern & Svensson (1996) takes place, then a dispersion in the fluence of a few orders of magnitude seems natural. The GRB itself emits just a fluctuating fraction of the total available energy, and probably there are many events where an observer sees no GRB. The pulse avalanche model describes the transmission of energy from a main reservoir as a highly unstable near-critical process, where in the idealized case of exact criticality and infinite available energy, the fluence distribution should become a power law.

A better candidate for the standard candle would be a single pulse independently of whether it alone constitutes a burst or appears as one of the pulses in a complex bursts. Again,

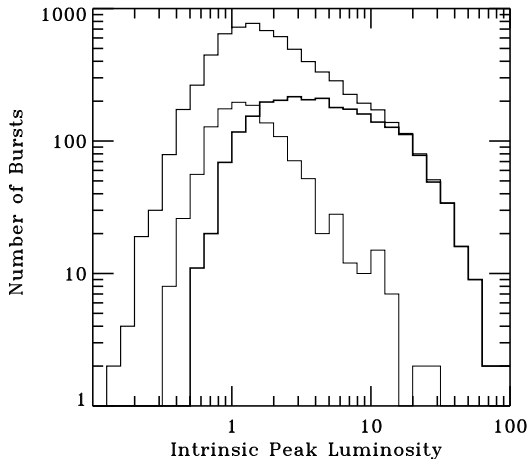


Fig. 6.— Example of intrinsic peak luminosity function for 7000 events simulated with the pulse avalanche model (upper curve). The peak amplitudes, p , of individual pulses were sampled with a log-normal distribution, $dn/dp \sim \exp[-\log^2 p/2\sigma^2]$ with $\sigma = 0.7$. Lower curves are peak distributions for simple (thin histogram, 1240 events) and complex (thick histogram, 2481 events). The separation of simple and complex events was obtained using the same procedure as described in § 3.1 rescaling simulated bursts to the same peak count rate, 55 counts/64 ms. GRBs with $\tau_r + \tau_d < 2$ s and those that did not pass the trigger were not used in the classification procedure. The χ^2 distribution for simulated events is more sharply peaked at $\chi^2 \sim 1$ than was the case for real events.

the distribution of the pulse peak amplitudes (fluxes) within one GRB seems narrower than the distribution of the pulse fluences (for studies of the fluence distribution of pulses in GRBs, see Li & Fenimore 1996) – otherwise a negative correlation between the pulse duration and its amplitude within one GRB would be visible. Does any correlation exist within one event? The visual impression from GRBs time profiles is that there is no evident correlation. Unfortunately such a correlation is not easy to extract as pulses tend to overlap and it is very easy to take a dense bunch of narrow pulses for a single pulse.

Actually the peak amplitudes should be distributed somehow. Let us consider, as an example, a log-normal distribution for the pulse peak amplitude (the same distribution was found by Li & Fenimore 1996 for pulse fluences). Using this distribution in the pulse avalanche simulations we determined the corresponding intrinsic peak luminosity function for the simulated bursts caused by the piling up of pulses. We then applied the same procedure of χ^2 selection to our simulated bursts that was used to separate simple and complex real GRBs (see §3.1). The difference in the distributions of intrinsic peak luminosities of simple and complex events in this example (see Fig. 6) seems sufficient to cause a difference in the behavior of their $\log N - \log P$ curves in the presence of a strong evolutionary effect (the ratio of the median peak flux of the distributions is 3.7).

6. SUMMARY AND CONCLUSIONS

The effects we confidently detect can be summarized as follows:

1. Complex bursts have systematically larger peak count rates than simple bursts. Their peak count rate distribution has an apparent break at a count rate ~ 200 counts/64 ms which exceeds the threshold by a factor four.
2. Weaker bursts have a stronger asymmetry between the rising and decaying slopes of the average time profile.
3. The weakest bursts have a different shape of the average time profile, which can be described as a larger stretched exponential index (at least for the decaying slope).
4. The general temporal stretching of the ATP for weak bursts is complicated by the deformations of the ATP resulting from the two previous effects.

Effects 2) and 3) appear as direct consequences of effect 1). The effect 4) can be a superposition of both cosmological time dilation (Paczynski (1992)) and intrinsic luminosity - duration correlation (Brainerd (1994)). Effects 1) – 3) can appear only as a result of the correlation between temporal properties of GRBs and their intrinsic luminosity (if we discard as explanation an evolution of GRBs temporal properties with time which seems unnatural). The large value of these effects indicates that the intrinsic luminosity function is a wide one: comparable with the apparent brightness dispersion from the distance distribution. Therefore the $\log N - \log P$ curve can be a convolution of two functions of comparable dispersions.

Both the most confident and the most informative effect is the first one. There is no obvious source for such a high near-threshold bias (selective for complex events) to account for this effect. There is, however, a natural phenomenon that could account for it. As was already mentioned above, this could be the evolution of the star production rate. We must accept this as a possible explanation if we accept the merging of neutron star binaries as the source of GRBs.

It seems that we succeeded to extract an intrinsically strong subsample from the BATSE GRBs which covers distances to redshifts of $z \sim 1.5$ where evolutionary effects should be strong. A cosmological fit with an evolutionary factor for GRBs based on the measured star formation rate and with a model luminosity function similar to that presented in § 5 is a matter for separate work. The crucial data to confirm this point of view could appear from the search for untriggered bursts in the continuous BATSE data records. This search is ongoing (Kommers et al. 1997) and is worth intensifying.

We thank Felix Ryde for helpful assistance. This study made use of the data provided by the Compton Observatory Science Support Center. We are grateful to the BATSE team for a fast supply of new data to the publically available database. This research was supported by grants from the Swedish Natural Science Research Council, Stockholm University, the Swedish Royal Academy of Sciences, the Wenner-Gren Foundation for Scientific Research and a NORDITA Nordic Project grant.

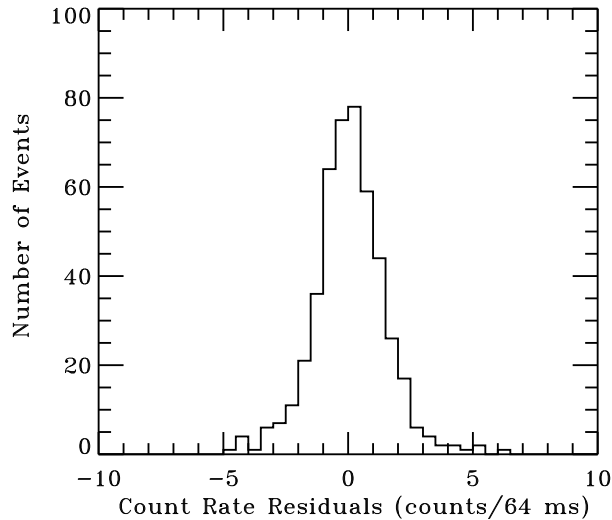


FIG. 7.— Residuals of our background fits in “testing windows” located in time intervals where the contribution of the GRB is invisible. The background fits were obtained using “fitting windows” (see text).

APPENDIX

A. DATA ANALYSIS

A.1. Background Fitting

The background fitting was based on a visual scan of all BATSE bursts. This work cannot be done automatically because there exist many events with complex backgrounds contaminated with non-Poisson features which can mimic the contribution of a GRB. In fact, each individual burst requires a researcher’s decision – how to fit it or whether it should be discarded. To avoid subjective biases for weak events, we followed the rules described below:

1. All fits are linear (the background anyway often demonstrates a non-polynomial behavior and a higher order polynomial fit could be unstable). Linear fits were made over one or two “fitting windows”, which were set in “quiet” time intervals, having a good χ^2 . We also set the “observational” windows avoiding background features not associated with the burst. In the case of a smooth curved background with several burst episodes in the event, we set a few fitting windows including quiet time intervals between burst episodes, so the background was approximated by a broken line.

2. Each feature separated by a wide time interval from the main peak should be tested whether it came from the same direction as the main peak. To compare directions we made a linear fit to the count rate in each of eight LADs in the time interval covering the feature. We then maximized the total reduced χ^2 in the time interval varying the time resolution, and calculated the eight-component vector χ^2 . This vector should approximately be parallel to that of the main peak, otherwise the feature should be avoided when setting the observational windows. The procedure turned out to be an efficient way to clean up bursts from unrelated fluctuations.

3. We adopted a default set of windows: a fitting window (-120 s – -70 s, where the boundaries are given relative to the trigger time), an observational window (-70 s – $+200$ s), and a second fitting window ($+200$ s – $+250$ s). If possible, we used the default set. If the background has a moderate curvature, it should not give a bias as it has a random sign. This rule reduces a possible subjective bias. A narrower time interval between the fitting windows was allowed if the burst was apparently short or if the background was strongly curved.

4. All events, where we were unable to make a confident conclusion that we did not lose and did not contaminate the signal at 100 s after and 50 s before the highest peak, were discarded. This could be due to wide data gaps, strong solar flares, rapid variations of the background, or chaotic variations with bad χ^2 from the wrong direction.

This fitting procedure gives as small bias as possible when summing up signals from different GRBs to get the average time profile, despite the fact that it is not accurate when dealing with individual events. To estimate the magnitude of possible errors introduced by the fitting procedure we made the following test. For each event where it was possible ($\sim 75\%$ of all events), we selected testing windows between our fitting windows avoiding regions with GRBs signals and measured the residuals of our fits in the testing windows. The distribution of residuals for 469 weak and medium events is shown in Figure 7. The distribution of residuals is reasonably symmetric, the average value for the residual is $+0.084$ counts/64 ms, the 1σ variance is 1.43 counts/64 ms. This is an argument that we have no significant systematic error (that exceeds the statistical error). The statistical error for the average residual is 0.11 counts/64 ms. For comparison, the typical background in channels 2 and 3 is 300 counts/64 ms, the peak count rate for the weakest events is ~ 50 counts/64 ms. The error introduced into the average time profile is inversely proportional to the peak count rate. For medium and bright events we can neglect the fitting uncertainty – it is much less than 10^{-3} . The exception is the weakest group where the 1σ error in the relative averaged residual is 1.5×10^{-3} .

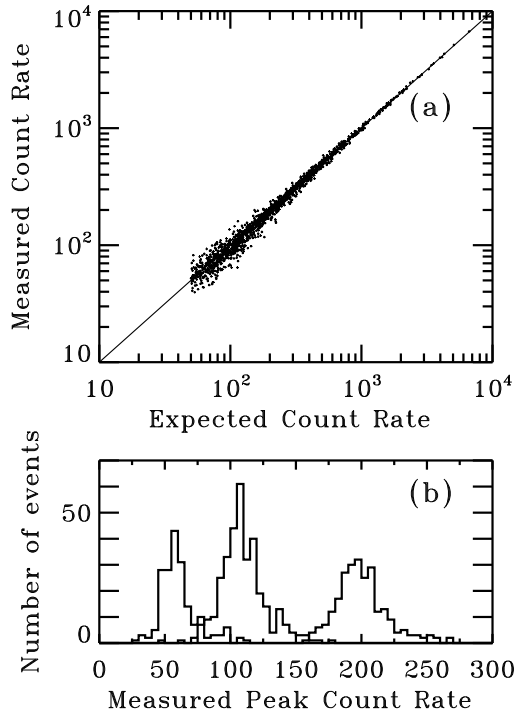


FIG. 8.— Test of the procedure for the peak count rate estimate. a) expected vs. measured count rate scattering plot obtained with bright events longer than 2 s rescaled to lower brightness. Note that the peak count rate estimate is based on the 64 ms resolution. b) Distributions of the measured peak count rates at fixed expected count rate P : $P = 55$ counts/64 ms; $P = 110$ counts/64 ms; $P = 200$ counts/64 ms. Bursts which did not pass the simulated trigger are not included. For description of rescaling and triggering procedures, see § A.3.

A.2. Selection of the Highest Peak

The direct peak selection using the highest 64 ms bin, while working good for bright events, suffers from Poisson noise for weak events. It just takes the highest Poisson fluctuation as being the burst’s highest peak. Nevertheless, as far as we adopted the 64 ms resolution approach, we should not use a different time resolution for weak bursts. As a compromise, we developed a hybrid scheme which combines a search for the peak interval in a lower time resolution and a search for statistical significant deviations in this interval with a higher time resolution.

First, we determine the shortest time-scale, $\Delta t_j = 64 \text{ ms} \times 2^j$, $j = 0, \dots, 4$, where a GRB has statistically significant variations between neighboring time bins (a 7σ threshold, which corresponds to a 5σ threshold for a deviation from the average). Then we search for the highest peak centered at bin number k using the time resolution, Δt_j , and calculating the peak flux as $\max\{\sum_i c(i) \exp[-((k-i)/2^j)^2]\}$ where k and i are indices of 64 ms bins, and $c(i)$ is the count rate in the i -th bin.

Then, if $j \geq 1$ we make a second iteration: searching for statistically significant excess over average within the brightest Δt_j interval using a shorter time-scales. The significance threshold, h_l ($l < j$), is reduced at this step. The thresholds were optimized empirically when tuning the scheme by rescaling strong bursts to the weakest, adding corresponding Poisson noise, selecting the highest peak, and comparing resulting peak amplitude and position with true values. With thresholds $h_0 = 4.0\sigma$, $h_1 = 3.2\sigma$, $h_2 = 2.0\sigma$, and $h_3 = 1.2\sigma$ above the average count rate in Δt_j we obtain a reasonable linearity between the expected and the measured count rate and still preserve the 64 ms resolution.

A test of this procedure by rescaling strong events to a given value of peak count rate is presented in Figure 8. The rescaling procedure is described in § A.3. Only those events which passed our simulated trigger after rescaling were included into the test distributions. One can see from Figure 8a that we have a reasonable linearity between the measured and the expected peak count rates (compare with a similar plot in Fig. 2 of in ’t Zand & Fenimore 1994). The systematic bias in the peak count rate for the weakest events is within 3%, the relative error is $\sim 35\%$ (FWHM) for $P = 55$ counts/64 ms and $\sim 22\%$ for $P = 110$ counts/64 ms. There are non-Gaussian tails towards higher values associated with Poisson fluctuations. They, however, do not exceed a few per cent of the peak integral. If one increases the thresholds, these tails will disappear, but a nonlinear bias of peaks towards lower values will appear. The thresholds have been set so as to have a reasonable average linearity of peak count rate estimates for weak events. (Note that direct selection of the highest bin in 64 ms resolution systematically overestimates the peak amplitude by a factor of 2 for the weakest events). The errors in the peak position can be characterized as follows: in 35% of the cases, the error does not exceed one 64 ms bin, with 47% probability the error is within 0.128s, with 83% probability it is within 1s, and in 6% of the cases the error exceeds 3s.

A.3. The Estimation of the Trigger Efficiency

We estimated the trigger efficiency assuming that GRBs of near-threshold count rate do not differ in their temporal properties from stronger GRBs (which is not exactly true). The procedure consists of the following steps:

1. For a given peak count rate P_0 , sample randomly one of the stronger bursts with a peak count rate $P > P_0$ of the same class (i.e., simple or complex) for which we are going to estimate the trigger efficiency and subtract the background thus extracting a

pure signal.

2. Sample randomly another strong event of arbitrary class in order to use its linear background fit.

3. Rescale the signal by factor P_0/P and distribute it between the two detectors having the largest projected areas for a randomly sampled direction of the burst. Distribute the signal proportionally to their projected areas. This step does not take into account the reflection from atmosphere which causes more uniform exposure of the detectors thus enhancing the trigger efficiency. The procedure also ignores the dependence of the detector response matrix on the projection angle. This dependence also enhance the trigger efficiency. Thus, our procedure slightly underestimates the trigger efficiency. It also neglects the probability of triggering three detectors for weak bursts.

4. Add a new linear background from two arbitrary detectors of the event sampled at step 2 and a corresponding Poisson noise (taking into account that some noise is already there in the rescaled signal).

5. Try the trigger procedure to the rescaled burst as it is programmed in BATSE (with the 5.5σ threshold that was used most of the observational time, see Meegan et al. 1998).

The fraction of rescaled bursts triggered with this procedure is the trigger efficiency. Note that with such a procedure the trigger efficiency is a function of the *expected* count rate.

A.4. Robustness of the ATP: Test for Brightness Dependent Biases

Brightness dependent errors in the ATP induced by Poisson noise are:

- Errors in the peak count rate estimate which is used as the normalization of a time profile,
- Errors in the peak position,
- Trigger selection effects which removes short or short spike dominated events from the sample.

We estimated the brightness dependent deformations of the ATP by rescaling strong events to low peak count rates and applying simulated trigger selection to the rescaled sample. The parent sample included 353 GRBs with the highest peak count rates of all morphologies and durations. The results are presented in Table 4 and in Figure 9.

TABLE 4
TIME CONSTANTS MEASURED WITH $\nu = 1/3$ FOR DIFFERENT PEAK COUNT RATE

Peak counts	t_r	t_d	Trigger efficiency
Parent sample	0.32	0.43	1.00
250	0.31	0.42	0.97
150	0.31	0.42	0.83
110	0.32	0.44	0.71
75	0.33	0.47	0.57

NOTE. — Test for robustness of ATP slopes against brightness dependent effects. The parent sample consists of 353 GRBs with the peak count rate (in 64ms resolution) in the interval $500 - \infty$. Then it was rescaled to the count rates displayed in the first column. Note that all time constants are correlated as all of them have the same parent sample. Therefore the errors of Table 1 are not applicable here and the time constants for different peak count rates have small dispersion. When comparing with Table 1 one can use the approximate coefficient 0.0072 to translate peak count rates into peak fluxes with units $\text{ph s}^{-1} \text{cm}^{-2}$.

We can state that down to the sample 5 of Table 1 deformations of the ATP are negligible (the count rate 110 counts/64 ms is near the boundary between samples 5 and 6) and only for sample 6 (75 counts/64 ms) are they significant. Therefore we can measure the variation of the ATP slopes without the rescaling procedure which would have erased some information for the strong samples.

B. STRETCHED EXPONENTIAL FITS AND THEIR ERRORS

As was noted in Stern (1996), the main problem when fitting ATPs is the correlation of deviations in different time bins (the ATP is the sum of more or less smooth but very different curves). This means that one cannot rely on deviations of individual profiles in a χ^2 fit, especially when estimating the accuracy of this fit. In principle, a proper solution of the problem should exist and it should require an overall correlation matrix implemented into the maximum likelihood method, but we expect that such a solution is not an easy one. In Stern (1996), the errors were estimated using a number of smaller samples of bursts. The variance of the time constants derived from the smaller samples was then rescaled to larger samples as $1/\sqrt{N}$, where N is the number of bursts in a sample. With a limited statistics such a procedure can only give a very approximate estimate of the errors and is very unreliable if one uses it to estimate the statistical significance level of observed effects.

Following SPS97 we estimate the statistical errors using the pulse avalanche model simulations. Here we present further details of the procedure. For a description of the pulse avalanche model, see Stern & Svensson (1996). The general time-scale in the model is defined mainly by an upper cutoff for the pulse width distribution. It was tuned to get desirable time constants for the stretched exponential average time profiles. Another parameter that was varied is the “criticality index”, μ , which defines the Poisson average of baby pulses per parent pulse in the avalanche. At supercritical values of μ , the process diverges. Varying this index some finer features like the stretched exponential index and the rise/decay asymmetry of the average time profile could be tuned. We, however, varied μ mainly in order to test a possible model-dependency of the statistical errors.

We found that the rise/decay asymmetry of the ATP can be described better when we introduced a “global envelope”, to be more exact, an external time dependence for the criticality index, $\mu = \mu^0 \exp(-t/T)$, where the “global” time constant T is large

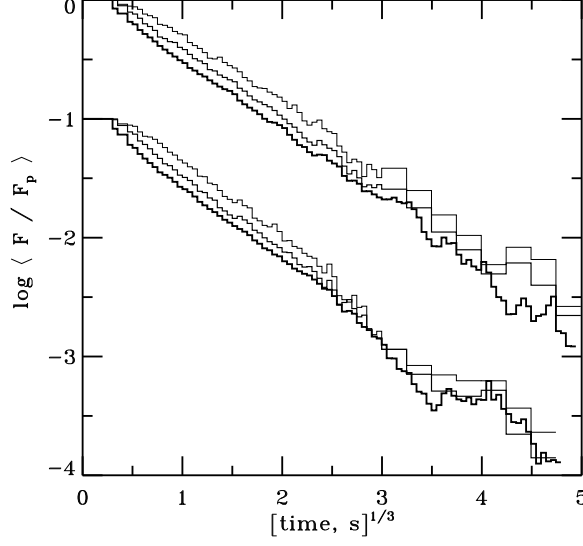


FIG. 9.— Deformations of the decaying (upper histograms) and rising (lower histograms) slopes of the ATP after rescaling of the parent sample of bright bursts. Thickest histograms: the ATP of the parent sample. Medium thick histograms: the ATP of the parent sample rescaled to a peak count rate of 150 counts/64 ms. Thin histograms: the ATP of the parent sample rescaled to a peak count rate of 75 counts/64 ms. The ATP of the parent sample rescaled to 250 counts/64 ms is almost indistinguishable from the parent sample.

($T = 400 - 600$ s). Then the main peak tends to appear earlier, the rise/decay asymmetry is therefore enhanced. Such a global envelope with a large time constant seems natural in many scenarios of GRB emission.

To fit the ATP one needs to split the ATP into a number of bins. This number should not be too large, otherwise neighboring bins will be too strongly correlated and the value of χ^2 or of other likelihood estimators would be completely meaningless. We choose equidistant binning in the $t^{1/3}$ scale, each bin being $0.25 \text{ s}^{1/3}$ wide. Correlations are still strong, but with a wider binning we could lose some information. Our value of χ^2 is still not usable as a direct estimator of the quality of the fit, but using the model we can calculate the distribution of χ^2 for many “intrinsically good” (i.e., giving a good stretched exponential at high statistic) ATPs and then define the actual effective number of degrees of freedom and the renormalization coefficient for χ^2 .

When fitting an ATP for a sample of N bursts, we must know how the deviations in each time bin are distributed for many independent samples. We calculated such distributions using $N \times K$ simulation runs which produce K independent samples of N events each (typically $K = 500$ and N vary from 100 to 1000). We found that the deviations are excellently described by a “continuous Poisson” distribution, or, in other terms, by a gamma-distribution: $\Phi(x, a) = a^x e^{-a} / \Gamma(x+1)$, where x is the distributed value, and a is a parameter equivalent to the Poisson average (traditionally gamma-distribution is used with a being the distributed value and $x - a$ a parameter).

We found that the Poisson average a in bin j for all studied cases can be parameterized as $a_j = p_j N \xi(p_j) \phi(p_j N)$ where p_j is the ATP value in the bin (averaged over $N \times K$ events), ξ and ϕ are slowly varying functions: ξ varies between 3 and 5, $\phi(x) = 1$ at $x > 2$ and smoothly decreases at $x < 2$. Then the standard maximum likelihood procedure was applied with an estimator $\chi^2 = -2 \sum_j \ln[\Phi(p_j - h_j, a_j) / \Phi(a_j, a_j)]$, where h_j is our hypothesis: $h_j = \beta \exp[-(t/t_0)^{1/3}]$. At large values of a_j , this expression coincides with the traditional χ^2 estimator.

We need two kind of fits depending on the aim. If we are interested in the shape of the ATP slope, we use a 3-parameter fit: $f(t) = \beta \exp[-|t/t_0|^\nu]$, where β , ν , and t_0 are free parameters with the additional requirement that β is close to 1 which is fulfilled in all reasonable cases. With pulse avalanche simulation runs (500×300) and (500×1000) we found that the error in the best fit estimate for ν is: $\sigma_\nu / \nu = 0.049 \times \sqrt{1000/N}$ where N is the number of events in the sample. The cross-correlation of t_0 and ν for a pulse avalanche simulation run (200×750) is shown in Figure 10. One can see that it is very strong and the error for t_0 is large for a free ν .

However, if we are interested in the behavior of time constants as a function of brightness we should fix ν . Indeed, we can compare time constants only with a hypothesis that the ATPs have the same shape (i.e., the same SE index ν) intrinsically. Our studies demonstrate that this hypothesis is not exactly true (see § 4). Nevertheless, the measurement of t_0 with constant ν is still the best that can be done. The deformation of the slope, if moderate, gives a second-order error. Therefore we measure t_0 with a 2-parameter fit.

In principle, one can set $\beta = 1$ and make a one parameter fit, but the first bin includes all possible biases from the finite resolution and the Poisson noise. We therefore excluded the first two bins ($t^{1/3} < 0.5$) from the fit treating β as a free parameter. The upper limit for the fitting range was set to $t^{1/3} = 5$ (i.e., $t = 125$ s).

As far as we have two slopes of the profile — pre-peak and post-peak, we fitted them simultaneously with different time constant, t_r (pre-peak, rising slope), t_d (post-peak, decaying slope), and a common β . Performing a number of model runs with different parameters, we found the accuracy of the stretched exponential fits to be almost model-independent. The standard deviation for the time constant does not change more than by 5% for different parameters and scales as $1/\sqrt{N}$ depending on the

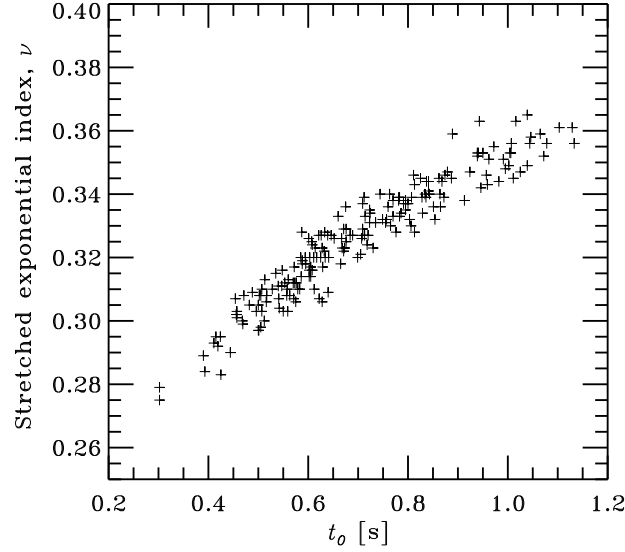


FIG. 10.— Scatter diagram for best fit values of stretched exponential index, ν , and time constant, t_0 , for pulse avalanche simulations.

number of events in the sample. The accuracy slowly increases, when the fitting time interval is extended (see Table 5). We chose the widest interval, which is the default for the results presented elsewhere in the paper.

TABLE 5
ACCURACY OF THE DETERMINATION OF THE TIME CONSTANTS WITH FIXED SE INDEX ν

Fitting interval	$\sigma(t_{r,d})/(t_{r,d}\sqrt{100/N})$
$0.125 < t < 8$	0.252
$0.125 < t < 27$	0.219
$0.125 < t < 64$	0.205
$0.125 < t < 125$	0.201

For the sum and ratio of time constants for pre-peak and post-peak slopes we have:

$$\sigma(t_r + t_d)/(t_r + t_d) = 0.196 \sqrt{100/N},$$

$$\sigma(t_d/t_r)/(t_d/t_r) = 0.135 \sqrt{100/N}.$$

Note, that the relative accuracy for the sum of time constants is close to that for one constant while the accuracy for their ratio is considerably better. This results from the strong correlation between the two slopes – a circumstance that favors the measurement of shape - brightness correlations and complicates the measurement of a time dilation effect.

As was mentioned above, the formal values of the χ^2 have no direct interpretation, the Pearson criterion does not work in this case because of strong correlations along the ATP. This could be interpreted as the effective (unknown) number of degrees of freedom being smaller than the numbers of bins. Actually the distribution of χ^2 becomes wider for a larger number of events in the sample. In Figure 11 we present two distributions of χ^2 for simulated samples which could be used for an approximate evaluation of the goodness of χ^2 obtained in the ATP fittings of real GRB samples.

REFERENCES

- Abraham, R. 1997, *Nature*, 387, 850
 Blinnikov, S. I., Novikov, I. D., Perevodchikova, T. V., Polnarev, A. G. 1984, *Sov. Astron. Lett.*, 10, 177
 Brainerd, J. J. 1994, *ApJ*, 428, L1
 Ching, E. 1991, *Phys. Rev. A*, 44, 3622
 Fenimore, E. E., & Bloom, J. S., 1995, *ApJ*, 453, 25
 Hartwick, F. D. A., & Schade, D. 1990, *ARA&A*, 28, 437
 in 't Zand, J. J. M., & Fenimore, E. E., 1994, in *Proc. 2nd Huntsville Gamma-Ray Burst Workshop* (New York: AIP), eds. G. J. Fishman, J. J. Brainerd, & Hurley K., p. 692
 Jensen, M. H., Paladin, G., & Vulpiani, A. 1992, *Phys. Rev. A*, 45, 7214
 Kommers, J. M., Lewin, W. H. G., Kouveliotou C., van Paradijs, J., Pendleton, G. N., Meegan, C. A., Fishman, G. J. 1997, *ApJ*, 491, 704
 Lee, T. T., & Petrosian, V. 1997, *ApJ*, 474, 37
 Lestrade, J. P. 1994, *ApJ*, 429, L5
 Li, H., & Fenimore, E. E. 1996, *ApJ*, 469, L115
 Lipunov, V. M., Postnov, K. A., Prokhorov, M. E., Panchenko, I. E., & Jorgensen, H. 1995, *ApJ*, 454, 593
 Madau, P., Ferguson, H. C., Dickinson, M. E., Giavalisco, M., Steidel, C. C., & Fruchter, A. 1996, *MNRAS*, 283, 1388
 Meegan, C. A., et al. 1996, *ApJS*, 106, 65
 Meegan, C. A., et al. 1998, *Current BATSE Gamma-Ray Burst Catalog*, <http://www.batse.msfc.nasa.gov/data/grb/catalog>
 Mitrofanov, I. G., Chernenko, A. M., Pozanenko, A. S., Briggs, M. S., Paciesas, W. S., Fishman, G. J., Meegan, C. A., & Sagdeev, R. Z. 1996, *ApJ*, 459, 570
 Mitrofanov, I. G., Litvak, M. L., & Ushakov D. A. 1997, *ApJ*, 490, 509

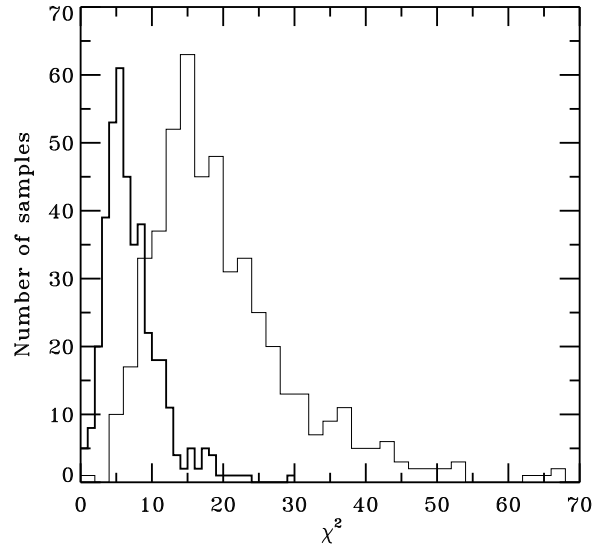


FIG. 11.— Examples of χ^2 distributions for simulated samples of GRBs. Thick histogram: 3-parameter fit of the decaying slope (free β , ν , and t_0), 1000 events in the sample, 15 formal degrees of freedom; thin histogram: 3-parameter simultaneous fit of both slopes of the ATP (free t_r , t_d , and a common β ; ν is fixed to 1/3), 300 events in the sample, 33 formal degrees of freedom.

Norris, J. P., Nemiroff, R. J., Scargle, J. D., Kouveliotou, C., Fishman, G. J., Meegan, C. A., Paciesas, W. S., & Bonnell, J. T. 1994, *ApJ*, 424, 540
 Norris, J. P., Nemiroff, R. J., Bonnell, J. T., Scargle, J. D., Kouveliotou, C., Paciesas, W. S., Meegan, C. A., & Fishman, G. J. 1996, *ApJ*, 459, 393
 Paczyński, B. 1992, *Nature*, 355, 521
 Pendleton, G. N., et al. 1997, *ApJ*, 489, 175
 Petrosian, V., & Lee, T. T. 1996, *ApJ*, 467, L29
 Prokhorov, M. E., Lipunov, V. M., & Postnov, K. A. 1997, in *Proc. XXXII Rencontres de Moriond, Les Arcs, France*, in press (astro-ph/9704039)

Stern, B. E. 1996, *ApJ*, 464, L111
 Stern, B. E., & Svensson, R. 1996, *ApJ*, 469, L109
 Stern, B. E., Poutanen, J., & Svensson, R. 1997, *ApJ*, 489, L41 (SPS97)
 Stern, B. E., Svensson, R., & Poutanen, J. 1997, in *The 2nd INTEGRAL Workshop: The Transparent Universe, St. Malo, France, Sept 1996*, ESA SP-382, 473